

# Break-up of an active chiral fluid

Luke Neville,<sup>1,2,\*</sup> Jens Eggers,<sup>1,†</sup> and Tanniemola B. Liverpool<sup>1,2,‡</sup>

<sup>1</sup>*School of Mathematics, Fry Building, University of Bristol, BS8 1UG, UK*

<sup>2</sup>*The Isaac Newton Institute for Mathematical Sciences, Cambridge CB3 0EH, UK*

We consider the non-linear dynamics governing the break-up of a two-dimensional strip of active chiral fluid. We observe that the strip thickness goes to zero at the pinch off points as a power law in finite time. Using slender body theory combined with a scaling analysis, we identify a new class of scaling exponents and scaling functions characterizing the speed and shape of break-up in these systems. The scaling analysis is in excellent agreement with direct numerical simulations of the hydrodynamic equations.

The formation of drops is familiar to us all, and can be seen when water pours from a kitchen tap [1, 2], or when wax rises in a lava lamp. In both examples, the driving mechanism is surface tension, which tries to reduce the surface area of the liquid by pinching off a drop [3, 4]. While the initial, linear dynamics of the water and wax look very similar, the non-linear dynamics just before break-up are quite different [5]. By studying droplet formation we are thus able to test the limits of different hydrodynamic theories by accessing their non-linear regime.

While the break-up dynamics of passive fluids are well understood [2, 3, 5], little is known when the fluid is *active*. Active fluids, which are comprised of particles that use energy to do work on their environment, show a variety of novel collective phenomena not seen in normal liquids [6, 7], and unlike passive fluids, may drive themselves unstable from the inside-out [6]. The effect of activity on interface dynamics has typically been studied in the linear or near-linear regimes. For example, small deviations from a flat interface [8] or in active phase separation [9, 10] determining the long-time scaling and size-distribution of stable droplets. Here, we look at the highly nonlinear dynamics right near break-up of an unstable active film.

In particular, we examine a new type of fluid break-up where the instability is not driven by surface tension, but rather the persistent spinning motion of the constituent particles [11–16]. These chiral active fluids behave much like ordinary fluids, except that they have anti-symmetric terms in their stress tensor that drive the local production of vorticity [17, 18]. The effect of these chiral stresses on break-up were demonstrated in recent experiments [11], on a two-dimensional incompressible chiral fluid, in contact with a substrate, made of millions of magnetic particles sedimented in water, and spun up by rotating magnetic fields [19]. Taking thin strips of this chiral fluid, they observed an asymmetric break-up into drops driven by counter-propagating edge currents at the strip boundaries (see Fig. 1(a)). A hydrodynamic theory and a linear stability analysis confirmed that the break-up was due to chirality. In this letter, we will go beyond the linear regime and study the fully non-linear

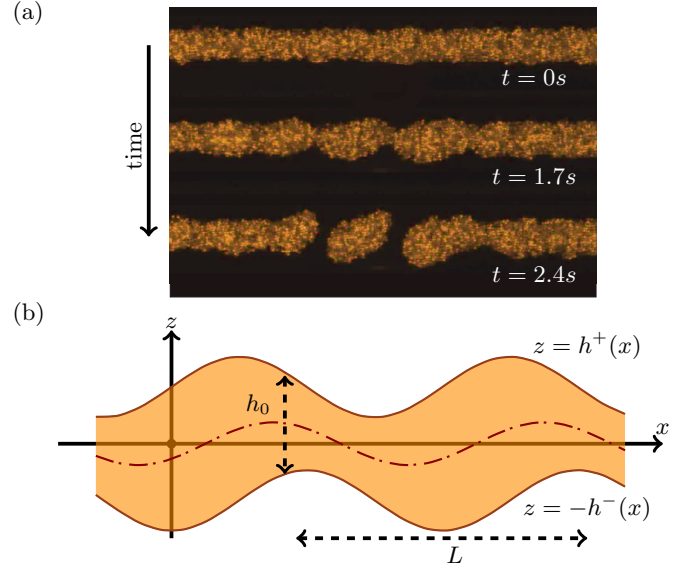


FIG. 1: (a) Experimental evidence of two dimensional strips of chiral fluid breaking up asymmetrically, adapted from Soni *et al.* [11]. The arrow marks the direction of time, with the strip going unstable before breaking up into drops. The whole process happens in only a few seconds. (b) Sketch of a strip of chiral fluid undergoing an instability leading to breakup. The top and bottom surfaces are at  $z = \pm h^\pm(x)$ , the characteristic vertical scale is  $h_0$ , the horizontal scale is  $L$ , and their ratio is  $\epsilon = h_0/L$ . The dot-dashed orange line marks the centerline of the strip at  $z = c(x)$ .

dynamics involved in break-up.

Using asymptotics based on the strips slenderness, we first derive one-dimensional equations for the strip evolution. Using these, we show that the strip evolves self-similarly near break-up, with the minimum thickness decreasing to zero as a power law in time. The corresponding exponent is not given by dimensional analysis, meaning we have self-similarity of the second kind [20]. The exponent and scaling function controlling the shape of the strip are determined through a scaling analysis, with our predictions perfectly matching results from our full PDE simulations.

*Hydrodynamics.*— Consider the strip of chiral fluid shown in Fig. 1. In the fluid bulk, inter-particle forces are balanced against the friction each particle feels from the the glass substrate. Using  $\boldsymbol{\sigma}$  for the stress tensor and  $\mathbf{u}$  for the velocity, this gives

$$\nabla \cdot \boldsymbol{\sigma} - \Gamma \mathbf{u} = \mathbf{0}, \quad (1)$$

where  $\Gamma$  is the friction coefficient of the substrate [11, 21, 22]. It is known [11, 23, 24], that these hydrodynamic stresses can be described by a modified Newtonian stress tensor

$$\sigma_{ij} = \eta(\nabla_i u_j + \nabla_j u_i) - p\delta_{ij} + \eta_R \epsilon_{ij}(2\Omega - \omega), \quad (2)$$

where  $\eta$  is the usual dynamic viscosity,  $p$  is the pressure, and  $\eta_R$  is the rotational viscosity [15]. The rotational viscosity term captures the friction felt whenever the spin rate of the particles,  $\Omega$ , is different to that of the surrounding water  $\omega/2 = \epsilon_{ij}\nabla_i u_j/2$  [23, 24]. In a passive system the conservation of angular momentum ensures these spin rates are equal and the rotational viscosity term vanishes. Indeed, switching off the magnetic field causes the magnetic particles to passively rotate at the same speed as the surrounding water.

At the strip boundaries the chiral fluid is free, and inter-particle stresses are balanced by surface tension to give

$$\boldsymbol{\sigma} \cdot \mathbf{n} = -\gamma(\nabla \cdot \mathbf{n})\mathbf{n}. \quad (3)$$

Here,  $\mathbf{n}$  is the unit outward normal to the chiral fluid,  $\gamma$  is the coefficient of surface tension [18, 25], and  $\nabla \cdot \mathbf{n}$  is (twice) the mean curvature of the interface. Note that the surface tension  $\gamma$  is not that of the surrounding water, but rather an effective tension arising from the magnetic attraction of each particle [11]. The experimentally measured values of all above parameters can be found in Soni *et al.* [11].

Using  $(x, z)$  for down and cross strip respectively, the top and bottom free surfaces have position  $z = \pm h^\pm(x)$  (see Fig. 1(b)), and evolve in time according to the kinematic boundary condition

$$h_t^\pm + u h_x^\pm = \pm v \Big|_{z=\pm h^\pm}, \quad (4)$$

where  $(u, v) = \mathbf{u}$ , and subscripts denote derivatives. For a passive fluid we would expect the strip to evolve symmetrically with  $h^+ = h^-$ , but chiral stresses break this symmetry. For later use we note that the height functions are related to the strip center-line and half-thickness by  $c = (h^+ - h^-)/2$  and  $h = (h^+ + h^-)/2$  respectively.

*One-dimensional reduction.*— To understand chiral break-up we must tackle the non-linear dynamics of  $h^\pm$  contained in equations (1), (3), and (4). This can be difficult even with a sophisticated numerical method like

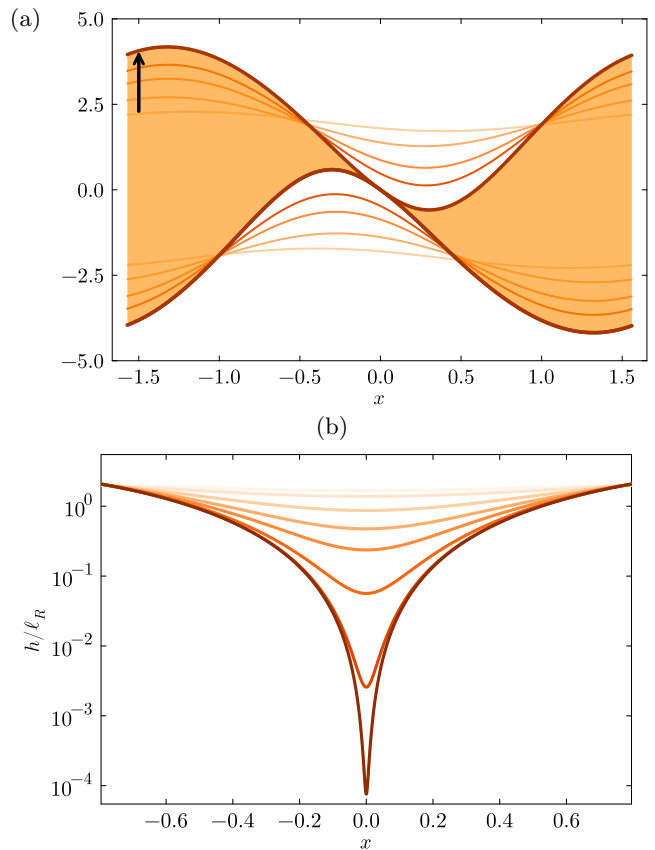


FIG. 2: (a) Numerical solution of equations (5) over a periodic domain of length  $\pi\ell_R$ . The light orange line shows the initial profile, and the sequence of darkening lines show the strip as time progresses. The black arrow indicates the direction of time. (b) The thickness function  $h$  remains symmetric about  $x = 0$  as time progresses. As the singularity is approached the minimum strip thickness decreases until pinch off when it becomes zero. In both plots lengths are measured in units of  $\ell_R = \gamma(\eta + \eta_R)/(\eta\eta_R\Omega)$ .

finite element. We will take an alternative approach, exploiting the slenderness of the strip to project the dynamics down into one dimension [3, 5, 26–29].

One-dimensional reductions have proven extremely successful in other problems [26, 27, 30], and follow the ideas of slender-body theory, expanding the dynamics in a small parameter characterising the strip aspect ratio. Leaving the derivation to the SI [31], we find

$$\begin{aligned} \Gamma c_t &= -\frac{4\eta\eta_R\Omega}{\eta + \eta_R} \frac{h_x}{h} + \gamma \frac{c_{xx}}{h}, \\ \Gamma h_t &= -\frac{4\eta\eta_R\Omega}{\eta + \eta_R} [hc_x]_{xx} + \gamma [c_x c_{xx} - h h_{xxx}]_x, \end{aligned} \quad (5)$$

which are two equations for the strip center-line and thickness. Keeping the parameters makes clear the origin of each term—those proportional to  $\Omega$  come from the

chiral stress, while others proportional to  $\gamma$  come from surface tension. Linear stability analysis of Eqns. (5) reproduces, at small wavenumbers, exactly the same behaviour as the full equations [11].

While a stability analysis shows that equations (5) capture the linear regime, we must numerically integrate them to understand non-linearities. Our simulations were done with periodic boundary conditions, using a well tested finite difference method [5, 26, 32]. Spatial derivatives were approximated to second order on a highly refined grid, that is adapted to scale with the pinch-region. We integrate forwards in time with a fully implicit step-halving method, ensuring both stability and second-order accuracy in time [33].

An example of non-linear evolution is shown in Fig. 2(a), where the initial shape is drawn in light orange, and a sequence of darkening lines shows the strip as time progresses. The final shape, which we fill in orange, pinches off at the origin. Somewhat surprising is that the thickness function  $h$  is symmetric about the pinch-point, with all asymmetry in the strip coming from the totally anti-symmetric center-line. The global (anti-)symmetry of these shapes is a result of the initial conditions, but were seen to hold true locally for all initial conditions we tried. The symmetry of  $h$  is demonstrated nicely in Fig. 2(b), which shows a sequence of thickness profiles as the break-up time is approached. Taking a closer look at Fig. 2(b) we notice that the break-up is highly localised, with the thickness decreasing rapidly near the origin but changing slowly in the far-field. This suggests that a local analysis of the pinch region will be sufficient.

*Scaling theory.*— The natural length and time scales for break-up are found from Eqns. (5) as  $\ell_R = \gamma(\eta + \eta_R)/(|\Omega|\eta\eta_R)$  and  $t_R = \ell_R^3\Gamma/\gamma$ , respectively. Measuring dimensionless distances and times to the pinch-point at  $(x_0, t_0)$  with  $x' = (x - x_0)/\ell_R$  and  $t' = (t_0 - t)/t_R$ , we will assume the dynamics to be self-similar as  $t', x' \rightarrow 0$  [5], with

$$\begin{aligned} h(x, t) &= \ell_R t'^{\alpha} f(x'/t'^{\beta}), \\ c_x(x, t) &= -S + t'^{\alpha_2} g(x'/t'^{\beta}). \end{aligned} \quad (6)$$

The power law pre-factors tell us that the strip thickness should decrease to zero as  $t'^{\alpha}$ , with a universal shape given by the scaling function  $f$ . Following our simulation results we assume that the center-line slope tends to a constant value  $-S$ , with all spatial dependence sitting in a scaling function that rides on top [34]. Note that we could have written the scaling form in terms of the center-line itself, but using the center-line slope is simpler

As we are interested in the final stages of break-up, we substitute (6) into (5) and keep only the most dominant terms as  $t' \rightarrow 0$ . A dominant balance argument [35]

reveals these to be

$$\begin{aligned} 4f_{\xi} &= g_{\xi}, \\ \frac{1+\alpha}{4}\xi f_{\xi} - \alpha f + (ff_{\xi\xi\xi})_{\xi} &= 0, \end{aligned} \quad (7)$$

where the similarity variable  $\xi = x'/t'^{\beta}$ ,  $\alpha_2 = \alpha$ , and  $\beta = (1 + \alpha)/4$ . All other choices of  $\beta$  and  $\alpha_2$  are inconsistent, being less dominant as  $t' \rightarrow 0$ . The exponent  $\alpha$  remains undetermined by dominant balance, but is found later by solving the non-linear eigenvalue problem (8) [20].

The terms in equation (7) come from a balance of chirality and tension in the center-line equation. The time derivative term is negligible, and thus the center-line is quasi-static in the pinch region. The second equation (8) comes from balancing the time-derivative and the surface-tension terms in the thickness equation, and interestingly is equivalent to the Hele-Shaw equation when converted to similarity variables [32, 36]. In the ordinary Hele-Shaw problem true self-similarity is never seen as the full equation in  $(x, t)$  variables is stable unless driven from the boundary [32, 37, 38]. Here, the linear instability set in by the chiral stress is enough to kick-start break-up and a true similarity solution is seen.

To find  $g$  we integrate equation (7), giving

$$g = 4f + g_0, \quad (9)$$

where  $g_0$  is a constant, zero in all our simulations. The center-line and thickness are hence characterised by the same scaling function  $f$ , which solves Eq. (8). This equation is fourth order with one free parameter, meaning five boundary conditions are required for a unique solution. Assuming symmetry about the pinch at  $\xi = 0$  yields the first three

$$f(0) = 1, \quad f_{\xi}(0) = 0, \quad f_{\xi\xi\xi}(0) = 0, \quad (10)$$

where we have used a scale-invariance of Eq. (8) to set the value at the origin to unity. The remaining degrees of freedom are the exponent  $\alpha$  and second derivative at the origin  $f_{\xi\xi}(0)$ , which parametrise a two-dimensional solution-space. A unique solution is picked from this by enforcing the matching condition

$$f \propto \xi^{\alpha/\beta} \quad \text{as} \quad |\xi| \rightarrow \infty, \quad (11)$$

which ensures that the thickness becomes static far from the pinch region, with  $t'$  dropping out of the scaling forms as  $\xi \rightarrow \infty$  [5]. As shown in the SI [31], matching corresponds to two conditions at infinity, and so Eq. (8) is now fully specified. The resulting problem is solved with the shooting method, yielding

$$\alpha \approx 1.2392, \quad f_{\xi\xi}(0) \approx 2.7789, \quad (12)$$

as well as the solid red curve in Fig. 3(b). Comparing this scaling with results from our PDE simulations in Fig. 3(a)

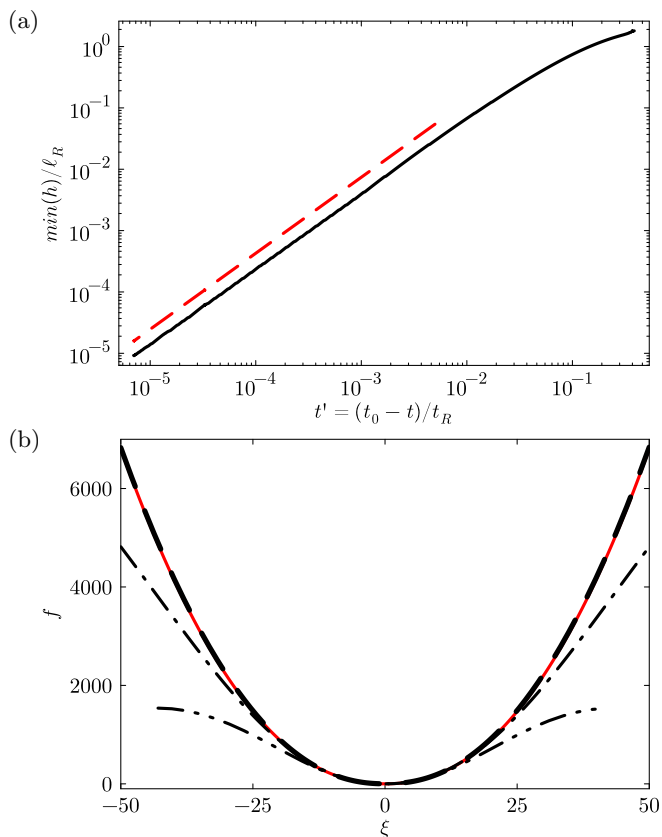


FIG. 3: (a) Scaling of the minimum strip thickness as a function of the time to break-up,  $t'$ . The black line is from the PDE simulation, and the red dashed line is the power law  $t'^{1.24}$ . (b) The scaling function  $f$ . The solid red line gives the prediction from our scaling theory; the dashed, dot-dashed, and chain-dashed lines come from the PDE simulation at  $t' = 7 \times 10^{-6}, 1.8 \times 10^{-4}, 7 \times 10^{-4}$ . The agreement between the PDE results and theory improves as break-up is approached.

we see excellent agreement, with the strip thickness going to zero like  $t'^{1.24}$ . The scaling function found from shooting also matches simulations, with the PDE results shown as dashed lines in Fig. 3(b) collapsing onto the predicted red curve as  $t' \rightarrow 0$ .

Our scaling analysis leads to the following understanding of chiral break-up. The initial linear instability sets the system in motion and twists the center-line, resulting in a center-line-slope grows like  $x^k$  for positive  $k$  far away from the pinch. The balance of chiral and surface tension forces in (7) means that the thickness also grows, with  $h \sim x^k/4$ . Substituting this into (8) we see that the power law causes a surface-tension driven mass current that grows like  $k(k-1)(k-2)x^{2k-3}$ , pumping fluid out of the pinch only if  $k > 2$ . This agrees with the results from our scaling theory, as the matching condition (11) gives  $k = \alpha/\beta \approx 2.2$ .

To conclude, we have studied the asymmetric break-

up of a strip of active chiral fluid using both asymptotics and simulations, showing that the strip thickness goes to zero as a power law in finite time with a new class of exponents. While odd-viscosity was not required to explain the experimental results that motivated this study [11], it could be added to our picture if needed. A related problem to the one we have studied here is the coalescence of chiral droplets [11]. We leave all this for future work.

*Acknowledgements*—TBL, LN would like to thank the Isaac Newton Institute for Mathematical Sciences, Cambridge, for support and hospitality during the programme *New statistical physics in living matter*, where part of this work was done. This work was supported by EPSRC grants EP/V520287/1, EP/R014604/1 and EP/T031077/1. LN acknowledges the support of an EPSRC studentship and thanks Henry Andralojc for many interesting discussions, and for help in understanding the symmetries of the problem.

\* [luke.neville@bristol.ac.uk](mailto:luke.neville@bristol.ac.uk)

† [jens.eggers@bristol.ac.uk](mailto:jens.eggers@bristol.ac.uk)

‡ [t.liverpool@bristol.ac.uk](mailto:t.liverpool@bristol.ac.uk)

- [1] X. Shi, M. P. Brenner, and S. R. Nagel, A cascade of structure in a drop falling from a faucet, *Science* **265**, 219 (1994).
- [2] J. Eggers and E. Villermaux, Physics of liquid jets, *Reports on progress in physics* **71**, 036601 (2008).
- [3] J. Eggers, Universal pinching of 3d axisymmetric free-surface flow, *Physical Review Letters* **71**, 3458 (1993).
- [4] J. Eggers, Nonlinear dynamics and breakup of free-surface flows, *Reviews of modern physics* **69**, 865 (1997).
- [5] J. Eggers and M. A. Fontelos, *Singularities: formation, structure, and propagation*, Vol. 53 (Cambridge University Press, 2015).
- [6] M. C. Marchetti, J.-F. Joanny, S. Ramaswamy, T. B. Liverpool, J. Prost, M. Rao, and R. A. Simha, Hydrodynamics of soft active matter, *Reviews of modern physics* **85**, 1143 (2013).
- [7] S. Ramaswamy, The mechanics and statistics of active matter, *Annu. Rev. Condens. Matter Phys.* **1**, 323 (2010).
- [8] R. Adkins, I. Kolvin, Z. You, S. Witthaus, M. C. Marchetti, and Z. Dogic, Dynamics of active liquid interfaces, *Science* **377**, 768 (2022).
- [9] R. Singh and M. Cates, Hydrodynamically interrupted droplet growth in scalar active matter, *Physical review letters* **123**, 148005 (2019).
- [10] E. Tjhung, C. Nardini, and M. E. Cates, Cluster phases and bubbly phase separation in active fluids: reversal of the ostwald process, *Physical Review X* **8**, 031080 (2018).
- [11] V. Soni, E. S. Bililign, S. Magkiriadou, S. Sacanna, D. Bartolo, M. J. Shelley, and W. T. Irvine, The odd free surface flows of a colloidal chiral fluid, *Nature physics* **15**, 1188 (2019).
- [12] B. Liebchen and D. Levis, Chiral active matter, *Europhysics Letters* **139**, 67001 (2022).
- [13] M. Han, M. Fruchart, C. Scheibner, S. Vaikuntanathan, J. J. De Pablo, and V. Vitelli, Fluctuating hydrodynam-

- ics of chiral active fluids, *Nature Physics* **17**, 1260 (2021).
- [14] C. B. Caporusso, G. Gonnella, and D. Levis, Phase coexistence and edge currents in the chiral lennard-jones fluid, *Physical Review Letters* **132**, 168201 (2024).
- [15] S. Fürthauer, M. Stempel, S. W. Grill, and F. Jülicher, Active chiral fluids, *The European physical journal E* **35**, 1 (2012).
- [16] T. Markovich and T. C. Lubensky, Odd viscosity in active matter: Microscopic origin and 3d effects, *Physical Review Letters* **127**, 048001 (2021).
- [17] G. K. Batchelor, *An introduction to fluid dynamics* (Cambridge university press, 2000).
- [18] L. D. Landau and E. M. Lifshitz, *Fluid Mechanics: Volume 6*, Vol. 6 (Elsevier, 1987).
- [19] H. Massana-Cid, D. Levis, R. J. H. Hernández, I. Pagonabarraga, and P. Tierno, Arrested phase separation in chiral fluids of colloidal spinners, *Physical Review Research* **3**, L042021 (2021).
- [20] G. I. Barenblatt, *Scaling, self-similarity, and intermediate asymptotics: dimensional analysis and intermediate asymptotics*, 14 (Cambridge University Press, 1996).
- [21] L. L. Jia, W. T. Irvine, and M. J. Shelley, Incompressible active phases at an interface. part 1. formulation and axisymmetric odd flows, *Journal of Fluid Mechanics* **951**, A36 (2022).
- [22] S. Ramaswamy and G. F. Mazenko, Linear and nonlinear hydrodynamics of low-friction adsorbed systems, *Physical Review A* **26**, 1735 (1982).
- [23] A. Chaves, M. Zahn, and C. Rinaldi, Spin-up flow of ferrofluids: Asymptotic theory and experimental measurements, *Physics of Fluids* **20** (2008).
- [24] E. Kirkinis and M. Olvera de la Cruz, Activity-induced propulsion and separation of passive chiral particles in liquids, *Physical Review Fluids* **8**, 023302 (2023).
- [25] Y. Zhang, J. E. Sprittles, and D. A. Lockerby, Nanoscale thin-film flows with thermal fluctuations and slip, *Physical Review E* **102**, 053105 (2020).
- [26] J. Eggers and T. F. Dupont, Drop formation in a one-dimensional approximation of the navier–stokes equation, *Journal of fluid mechanics* **262**, 205 (1994).
- [27] P. Howell, Models for thin viscous sheets, *European Journal of Applied Mathematics* **7**, 321 (1996).
- [28] D. T. Papageorgiou, On the breakup of viscous liquid threads, *Physics of fluids* **7**, 1529 (1995).
- [29] T. Erneux and S. H. Davis, Nonlinear rupture of free films, *Physics of Fluids A: Fluid Dynamics* **5**, 1117 (1993).
- [30] W. W. Zhang and J. R. Lister, Similarity solutions for van der waals rupture of a thin film on a solid substrate, *Physics of Fluids* **11**, 2454 (1999).
- [31] See Supplemental Material at [URL will be inserted by publisher] which presents additional details.
- [32] A. L. Bertozzi, M. P. Brenner, T. F. Dupont, and L. P. Kadanoff, Singularities and similarities in interface flows, in *Trends and perspectives in applied mathematics* (Springer, 1994) pp. 155–208.
- [33] S. A. Teukolsky, B. P. Flannery, W. Press, and W. Vetterling, Numerical recipes in c, *SMR* **693**, 59 (1992).
- [34] J. Eggers, Singularities in droplet pinching with vanishing viscosity, *SIAM Journal on Applied Mathematics* **60**, 1997 (2000).
- [35] C. M. Bender and S. A. Orszag, *Advanced mathematical methods for scientists and engineers I: Asymptotic methods and perturbation theory* (Springer Science & Business Media, 2013).
- [36] J. Eggers and M. A. Fontelos, The role of self-similarity in singularities of partial differential equations, *Nonlinearity* **22**, R1 (2008).
- [37] T. F. Dupont, R. E. Goldstein, L. P. Kadanoff, and S.-M. Zhou, Finite-time singularity formation in hele-shaw systems, *Physical Review E* **47**, 4182 (1993).
- [38] R. Almgren, A. Bertozzi, and M. P. Brenner, Stable and unstable singularities in the unforced hele-shaw cell, *Physics of Fluids* **8**, 1356 (1996).

## Supplementary Material: Break-up of an active chiral fluid

Luke Neville,<sup>1,2,\*</sup> Jens Eggers,<sup>1,†</sup> and Tanniemola B. Liverpool<sup>1,2,‡</sup>

<sup>1</sup>*School of Mathematics, Fry Building, University of Bristol, BS8 1UG, UK*

<sup>2</sup>*The Isaac Newton Institute for Mathematical Sciences, Cambridge CB3 0EH, UK*

### DERIVING THE EQUATIONS

To derive the one-dimensional equations from the full hydrodynamics we introduce characteristic horizontal and vertical scales  $L$  and  $h_0$ , with ratio  $\epsilon = h_0/L$ . Assuming that this parameter is small, we non-dimensionalise all quantities according to

$$\begin{aligned} x &\sim L, & z &\sim \epsilon L, & h^\pm &\sim \epsilon L, \\ u &\sim u_0, & v &\sim \epsilon u_0, & p &\sim \frac{u_0(\eta + \eta_R)}{L}, \\ \sigma &\sim \frac{\eta u_0}{L}, & \gamma &= \frac{\eta u_0}{\epsilon} \tilde{\gamma}, & t &\sim \frac{u_0}{L}, \end{aligned} \quad (\text{S1})$$

where  $u_0$  is a velocity scale to be set later. The scaling of surface tension is chosen to ensure it comes in at leading order [27]. Substituting these into the Stokes equation, we pick a vertical scale  $h_0 = \sqrt{(\eta + \eta_R)/\Gamma}$  to ensure that friction comes in to balance viscosity. The resulting equations are

$$(\epsilon^2 \partial_x^2 + \partial_z^2)u - \epsilon^2 \partial_x p - u = 0, \quad (\text{S2a})$$

$$(\epsilon^2 \partial_x^2 + \partial_z^2)v - \partial_z p - v = 0, \quad (\text{S2b})$$

$$\partial_x u + \partial_z v = 0, \quad (\text{S2c})$$

where all variables and coordinates are now dimensionless.

Assuming that the velocity scale is set by the rotation rate of the cubes we choose  $u_0 = \Omega h_0$ , yielding non-dimensionalised stress components

$$\begin{aligned} \sigma_{xx} &= 2\partial_x u - p(1 + R), \\ \sigma_{zz} &= 2\partial_z v - p(1 + R), \\ \sigma_{xz} &= \epsilon^{-1}(1 + R)\partial_z u + \epsilon(1 - R)\partial_x v - 2R\epsilon^{-1}, \\ \sigma_{zx} &= \epsilon^{-1}(1 - R)\partial_z u + \epsilon(1 + R)\partial_x v - 2R\epsilon^{-1}. \end{aligned} \quad (\text{S3})$$

where  $R = \eta_R/\eta$  is the ratio of the rotational and dynamic viscosities. The dimensionless dynamic boundary condition is given by

$$\epsilon \boldsymbol{\sigma} \cdot \mathbf{n}^\pm = -\tilde{\gamma}(\nabla \cdot \mathbf{n}^\pm) \mathbf{n}^\pm, \quad (\text{S4})$$

while the kinematic condition remains the same.

We solve equations (S2) perturbatively in the small parameter  $\epsilon$ , expanding the fields as a series in  $\epsilon^2$ ,

$$\mathbf{u} = \mathbf{u}_0 + \epsilon^2 \mathbf{u}_1 + \dots, \quad (\text{S5a})$$

$$p = p_0 + \epsilon^2 p_2 + \dots, \quad (\text{S5b})$$

while assuming  $h^\pm$  are  $O(1)$ . At leading order for  $u_0$  we have

$$\partial_z^2 u_0 - u_0, \quad (\text{S6a})$$

$$\partial_z u_0 \Big|_{z=\pm h^\pm} = \frac{-2R}{1+R}, \quad (\text{S6b})$$

where the boundary condition comes from the balance of tangential stresses along the free surface. Solving these gives the zeroth order velocity as

$$u_0 = -\frac{2R}{1+R} \operatorname{sech}(h) \sinh(z - c). \quad (\text{S7})$$

Combing this with the incompressibility condition, the other component of the Stokes equation and the normal stress boundary conditions, we can compute  $v_0$  and  $p_0$ . The results are quite lengthy, but simplify tremendously when substituted into the kinematic boundary conditions (4). The resulting equations of motion for the center-line and thickness are

$$h_t = 0, \quad (S8)$$

$$c_t = -\frac{4R \operatorname{sech}(h)^2 h_x}{(1+R)^2 h} + \frac{\tilde{\gamma} c_{xx}}{(1+R)h},$$

where subscripts denote derivatives. The thickness remains quasi-stationary at this order, which we soon see is because its equation is higher order in a derivative expansion. Pushing the calculation to next order in  $\epsilon$  is conceptually easy, but technically difficult due to the complicated algebra. The next-order velocities and pressures were computed with mathematica and take many pages. Thankfully they simplify when plugged into the kinematic condition (4) to give

$$h_t = \epsilon^2 \left[ -\frac{4R c_x \tanh(h)}{(1+R)^2} + \frac{\tilde{\gamma} (c_x^2 + h_x^2 - 2h h_{xx})}{2(1+R)} \right]_{xx}, \quad (S9)$$

with the dynamics of the center-line given by (S8). The two equations (S8) and (S9) constitute a one-dimensional reduction of the full equations (1), (3), and (4), valid when the strip is slender. The equations of the main text are found by expanding the hyperbolic functions for small  $h$ , which is valid when the strip is thin, and then returning back to dimension-full coordinates.

We have checked that simulations of the full equations, including the hyperbolic functions obey the same scaling relations as the simplified equations from the main text.

## STABILITY AND SELECTION OF THE SIMILARITY EQUATIONS

In the main body of the text we stated that the solution depended on two parameters  $\alpha$  and  $f_{\xi\xi}(0)$ , and that they had to be tuned to satisfy the matching condition  $f \propto \xi^{\alpha/\beta}$  at infinity. The dependence on two parameters follows from calculating the power series expansion of  $f$  near  $\xi = 0$ . I.e. we substitute the expansion

$$f = 1 + \sum_{n=1}^{\infty} a_n \xi^{2n}, \quad (S10)$$

into the equation and solve for all the coefficients  $a_n$ . This can be done to arbitrarily high order using, say, mathematica, and it shows that all the coefficients depend on  $\alpha$  and  $a_1 = f_{\xi\xi}(0)/2$ . For example, the first two coefficients are

$$a_2 = \alpha/24, \quad a_3 = -a_1(1+5\alpha)/720. \quad (S11)$$

To demonstrate that a tuning of the two parameters amounts to a selection of the right solution we now perform a stability analysis, perturbing around the far-field behaviour by setting

$$f = \xi^{\alpha/\beta} + \delta P(\xi), \quad (S12)$$

and keeping terms linear in  $\delta$ . The perturbations  $P$  will fall into two classes: unstable perturbations that grow faster than  $\xi^{\alpha/\beta}$  at infinity, and stable perturbations that are constant or decay [5]. Although the perturbations  $P$  cannot be found exactly, a WKB analysis is sufficient to understand the stability at infinity. Upon substitution of  $P = e^\chi$  into the equation, we keep the most dominant terms as  $\xi \rightarrow \infty$  to get

$$\frac{1+\alpha}{4} \xi \chi' = -\xi^{\alpha/\beta} (\chi')^4, \quad (S13)$$

where  $' = \partial_\xi$ . Solving this equation we find four modes  $P_i = e^{\chi_i}$ , where

$$\chi_1 \sim \text{const.}, \quad \chi_2 \sim -\frac{3}{4} \left( \frac{1+\alpha}{4} \right)^{4/3} \xi^{4/(3+3\alpha)}, \quad (S14)$$

$$\chi_3 \sim \frac{3}{8} \left( \frac{1+\alpha}{4} \right)^{4/3} \xi^{4/(3+3\alpha)} (1 + \sqrt{3}i), \quad \chi_4 \sim \frac{3}{8} \left( \frac{1+\alpha}{4} \right)^{4/3} \xi^{4/(3+3\alpha)} (1 - \sqrt{3}i). \quad (S15)$$

The first mode  $P_1$  corresponds to a shift in the parameters of the solution. The second mode  $P_2$  is exponentially decaying at infinity and is stable. The remaining modes  $P_3$  and  $P_4$  are oscillatory, exponentially growing modes whose prefactors must be tuned to zero to hit the matching condition. Because the whole solution depends only on  $\alpha$  and  $a_1$ , this tuning is enough to select the solution in the main text.

Unfortunately the exponential growth is extremely weak, being approximately  $e^{\xi^{0.6}}$ . Numerically, this means we have to shoot to quite large values of  $\xi$  to attain convergence in  $\alpha$  and  $a_1$ .